Chapter 7

A case study

In this chapter an ultrasonic NDT situation from a Swedish nuclear power plant is considered. The aim is to demonstrate how mathematical modelling, as it has been developed in the previous chapters, may be used to optimize the inspection procedure through parameter studies. The choice of content is a result of fruitful discussions with people (at different levels) in the *Department for advanced NDE Services* at FORCE Institute. The content of the chapter is however solely the responsibility of the author.

In the first section the material component in question is presented and the adaption of the component to a form suitable for modelling is described. The last section contains the results of the parameter studies and a discussion of (the value of) these.

7.1 A model of the material component

The material component (or rather type) considered (the so-called s-weld) may be found in reactor 2 at the nuclear power plant in Oskarshamn and in reactor 1 and 2 at the nuclear power plant in Barsebäck, Sweden. On some of the main pipes in the water recirculation system, smaller bypass pipes are attached via bypass welds to a cone on the main pipe as shown in Fig. 7.1 (left). The figure shows part of a main pipe as well as a longitudinal cut of the attached bypass pipe. The component in question is shown in the thick rectangle(s) and has been blown up in the (unfortunately not very good) right figure. At the left of this figure, the upper part is the (isotropic) ferritic steel end of the cone on the main pipe. Below this, the coating (cladding) is seen, which prevents corrosion, heat damage etc. The buttering between the cone and the weld ensures a better contact. Finally, the anisotropic, inhomogeneous weld together with the bypass pipe of (isotropic) austenitic steel to the right are seen. The dimensions are given on the figure which is seen to be out of drawing. An important point is that due to the small separation between the weld and the sloping boundary of the cone, it is only possible to inspect the weld from the right side (bypass pipe) in the figure. Thus, in order to inspect for possible defects at the interface between buttering and cladding the elastic waves are required to penetrate the weld.

Mathematical modelling has previously been carried out for this component using the ray tracing technique briefly discussed in Chapter 2.6. In that activity, several examples of the component with corresponding macrographs of the weld were studied for setting up a mathematical model of the entire component. The final material model is shown in Fig. 7.2 with the different regions, separated by solid lines, labeled and properly scaled relative to

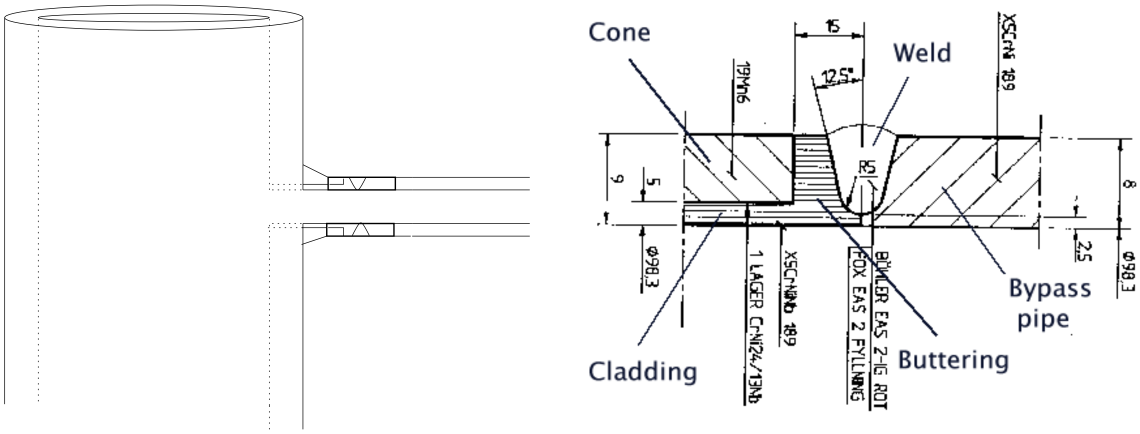

Figure 7.1: Illustrations of the material component considered. Left: A horizontal bypass pipe is attached to a main recirculation pipe through a bypass weld (the so-called s-weld) contained in the component marked out with thick lines. Right: Engineering drawing of the marked out component to the left.

the dimensions. Based on the macrographs a new region (F) being a separate weld was found and added. However, as indicated by dotted lines a few simplifications were made to this material model afterwards. Region D originally belonging to the buttering region was included in weld E to obtain a straight left sloping boundary. A straight right sloping boundary was furthermore constructed as indicated by neglecting the separate region F and including part of the lower weld in the isotropic region G. With these simplifications,

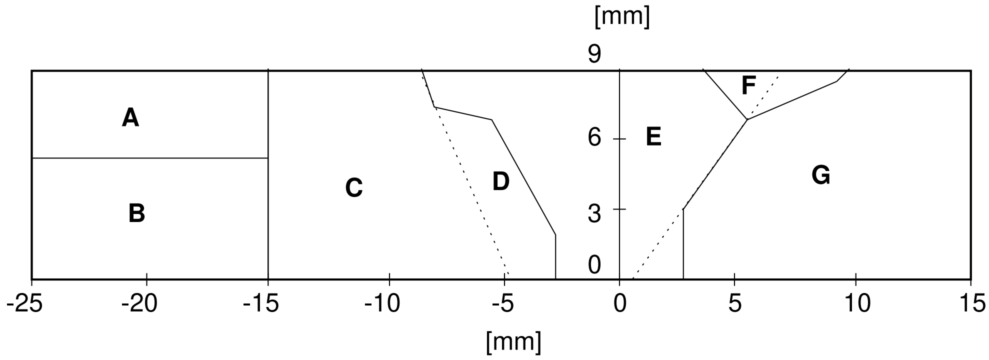

Figure 7.2: Original simulation model based on samples of the component in Fig. 7.1 (right). Regions are A: cone, B: cladding, C + D: buttering, E: weld 1, F: weld 2, G: bypass pipe. See text for simplifications of this model (indicated by dotted lines).

the weld model developed in the last chapter may straightforwardly be applied to this problem. As opposed to the examples considered in that chapter, the weld in this problem is highly asymmetric about the centerline. The various geometric parameters intering the weld model has been determined from Fig. 7.2. The parameters T_i and η have been determined by looking at the macrographs. The resulting grain model is shown in Fig. 7.3 with the parameter values listed in the legend.

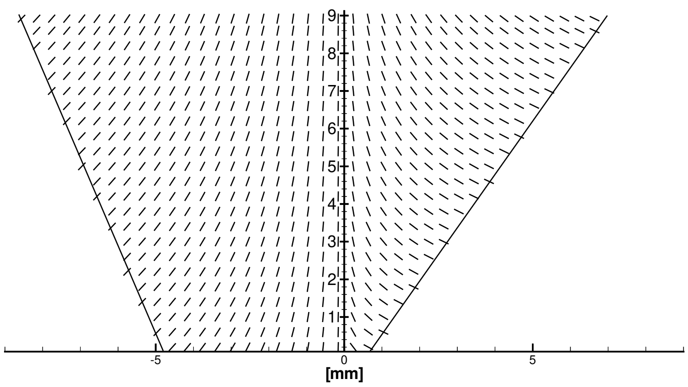

Figure 7.3: Grain orientations in the weld model in Fig. 7.2. Geometric weld parameters are $\alpha_1 = 35°$, $\alpha_1 = 23°$, $D_2 = 0.68$ mm and $D_1 = 4.8$ mm. Other parameters are $T_1 = 0.5$, $T_2 = 1.1$ and $\eta = 1.0$.

As the last point in this section, the material type and parameters for each region is specified. Region A is isotropic ferritic steel with a mass density $\rho = 8.02 \times 10^3$ kg/m^3 and elastic parameters and velocities

$$\begin{aligned} c_{11} &= 2.78 \times 10^{11}\,\text{Pa}, \qquad v_l = 5947\,\text{m/s} \\ c_{44} &= 0.823 \times 10^{11}\,\text{Pa}, \qquad v_t = 3236\,\text{m/s} \end{aligned}$$

The bypass pipe (region G) is considered to be isotropic austenitic steel with a mass density $\rho = 7.86 \times 10^3$ kg/m^3 and elastic parameters and velocities

$$\begin{aligned} c_{11} &= 2.67 \times 10^{11}\,\text{Pa}, \qquad v_l = 5770\,\text{m/s} \\ c_{44} &= 0.790 \times 10^{11}\,\text{Pa}, \qquad v_t = 3138\,\text{m/s} \end{aligned}$$

The cladding (B), buttering (C) and weld region (D+E) all consist of the transversely isotropic material X 6 CrNi 18 12 studied in detail in previous chapters and with elastic values given in Table 2.3, page 23. Without going into details, it is mentioned that the cladding and the buttering may be considered anisotropic and homogeneous. The homogeneity is a result of the manufacturing process. Regarding the cladding, the crystal symmetry axis is vertical, while the symmetry axis for in the buttering region is horizontal.

7.2 Parameter study

In the parameter study, it was decided to include a rectangular crack (with a stress-free surface) with a height of 2 mm and width of 0.04 mm to the left in the austenitic weld. The distance between the crack and the weld centerline is 4.6 mm. The situation is illustrated in Fig. 7.4. As transducer, a 60° L transducer with a width of 11 mm was used. Two frequencies, 2 MHz and 5 MHz, have been investigated. The length of the quadratic cells in the numerical simulation has been chosen as $\Delta x = 0.04$ mm. As mentioned earlier, this determines the size (and geometry) of the weld grains. The parameter investigated in the study was the distance X between the crack and the center of the transducer for both

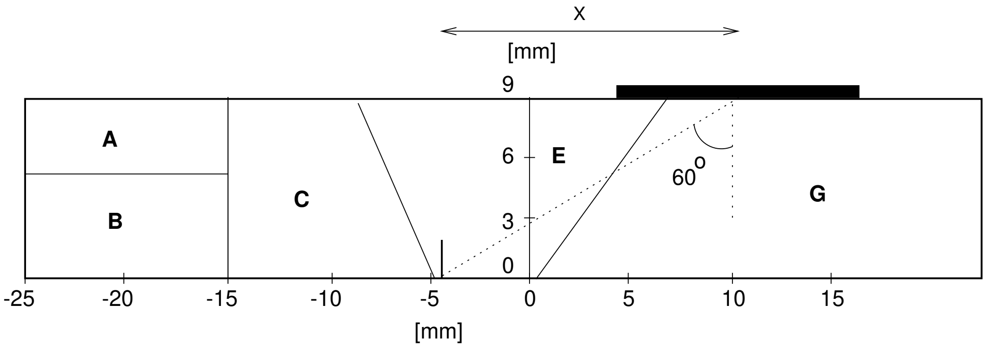

Figure 7.4: Illustration of the material model used in the parameter study.

choices of frequency. A-scans have then been obtained for a number of positions of the transducer on the component surface. In order to investigate the effect of the weld structure on the signal, A-scans were obtained both for the "true" anisotropic inhomogeneous austenitic weld and for the corresponding isotropic, homogeneous austenitic weld. A-scans have been reported relative to a SDH of diameter $\varnothing = 3\,\mathrm{mm}$ and with a center depth of 7 mm. For each A-scan, the diffracted echo from the upper crack tip as well as the corner echo from the bottom of the crack were of interest. Apart from the longitudinal wave, the additional transverse wave generated at the transducer with an angle of approximately 28° which is reflected at the backwall towards the crack where it is mode converted into a longitudinal wave propagating towards the transducer is also considered as it has a large amplitude.

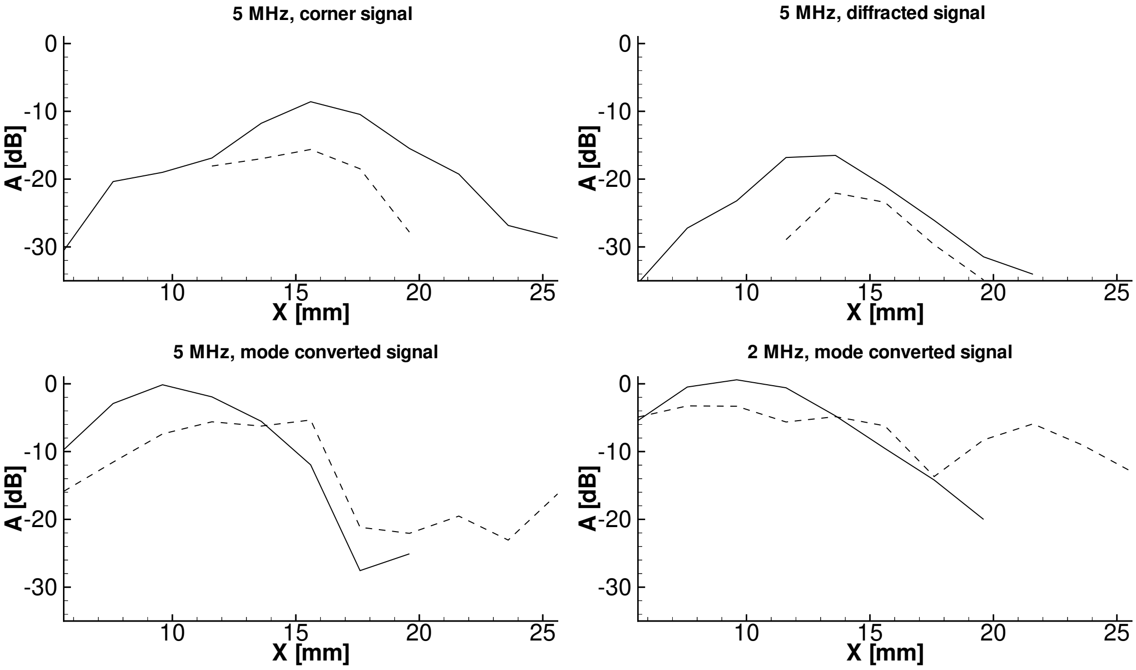

Figure 7.5: Results of the parameter study. See text for explanation.

The results of the parameter study are shown in Fig. 7.5 with dotted lines indicating the anisotropic austenitic weld and the full line indicating the isotropic austenitic weld. In the upper left plot, the corner signal from the crack bottom is shown. In the anisotropic case it was not possible to identify the corner signal and diffracted signal for small values of X due to the reflection of the qL wave on the backwall of the weld and for large values of X, the signal became too small. The optimal transducer positions, however, appear to be identical for the two material situations, $X \approx 15.6\,\mathrm{mm}$. To illustrate the influence of the weld on an entire A-scan, the corresponding two A-scans are shown in Fig. 7.6, with the relevant waves identified. In the upper right figure, the corresponding diffracted signal

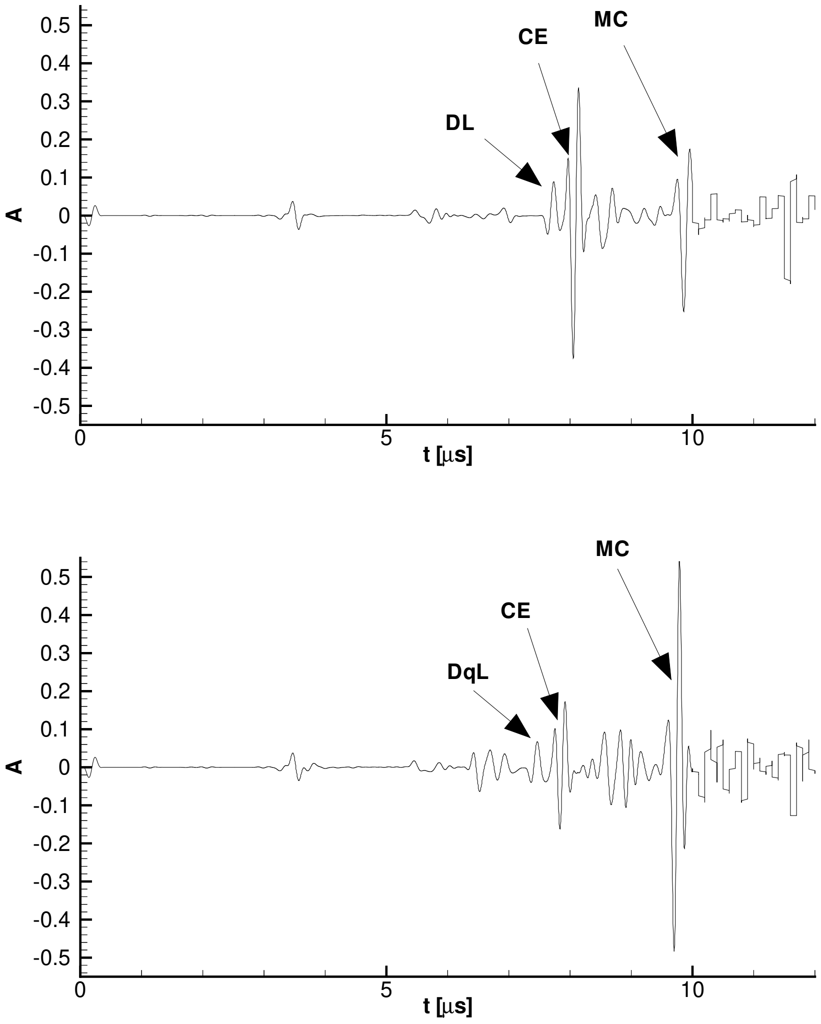

Figure 7.6: Examples of normalized A-scans for the isotropic case (upper plot) and anisotropic case (lower plot). Relevant waves are identified: Diffracted longitudinal (DL), corner echo (CE) and mode converted signal (MC). In both cases, $X = 15.6\,\mathrm{mm}$.

is shown with the same remarks as before. Note that the optimal transducer positions, which are not as uniquely defined as before, are translated with respect to the left figure. In the lower left plot, the mode converted signal is shown. In this case, it was easier to identify the signal in the anisotropic case for large values of X. The same situation is considered in the lower right plot but for the 2 MHz transducer instead. The signals in the last two plots resulting from the mode converted wave are seen to be rather strong. For the 2 MHz transducer it was not possible to separate the diffracted signal and the corner signal. Thus, this frequency is too small for this crack size. For most of the transducer positions examined, the signals in the isotropic, homogeneous material are the larger ones. Thus, some attenuation due to scattering takes place in the anisotropic, inhomogeneous weld. In a real situation the effect of scattering is much more pronounced, so the reported values should be considered as upper limits.

Concerning the A-scans, it was found that the interpretation of these was made much easier when studying a number of A-scans from nearby positions. To illustrate this, a number of A-scans for the isotropic weld are shown in Fig. C.1 and with the corresponding A-scans for the anisotropic weld shown in Fig. C.2, both normalized with respect to the reference SDH. This corresponds to the NDT operator moving the transducer back and forth on the surface for ease of interpretation. The two A-scans in Fig. 7.6 are identical to the lower plot in each of Fig. C.1 and Fig. C.2 respectively. See Fig. 7.6 for interpretation of echoes.

In conclusion, maximum amplitudes have been calculated as a function of transducer position along the surface. It is believed that such information may be valuable when determining optimal transducer positions for transmitting and receiving different types of waves. It was found that the presence of the anisotropic austenitic weld may result in different optimal transducer positions. The 2 MHz transducer considered was not suitable for detecting tip diffracted echoes as well as corner echoes. Furthermore, it was found that the backwall of the weld results in a major distortion of the diffraction echo as well as the corner echo. Obviously, this parameter study could be taken a lot further (including an improvement of the component model), but due to time restrictions, this was deemed appropriate as a demonstration of the usefulness of the developed simulation tool.